LANGMUIR

pubs.acs.org/Langmuir Article

Determination of Protein Charge in Aqueous Solution Using Electrophoretic Light Scattering: A Critical Investigation of the Theoretical Fundamentals and Experimental Methodologies

John F. Miller*

Cite This: https://dx.doi.org/10.1021/acs.langmuir.0c01694 Read Online

ACCESS | Metrics & More | Article Recommendations

ABSTRACT: Studies are reported of the measurement of electrophoretic mobilities of bovine serum albumin (BSA) in aqueous potassium chloride solutions as a function of ionic strength and pH using electrophoretic light scattering (ELS). It is demonstrated that the use of palladium or platinum electrodes should be avoided and that platinized platinum electrodes are necessary to avoid interference from unwanted electrochemical phenomena at the electrode−liquid interface. Potentiometric acid titration was performed to quantify the amount of protonic charge per protein molecule at the same pH values as the electrophoretic mobility measurements. It is shown that appropriate selection of an electrokinetic model yields excellent agreement between predicted and experimental electrophoretic mobilities across the ranges of pH and ionic strength studied in accordance with the protonic charge values obtained by titration. The experimental results are explained in terms of protonation, chloride counterion binding, and protein molecule permeability. This work highlights specific requirements of using ELS for confident analysis of proteins in aqueous solutions.

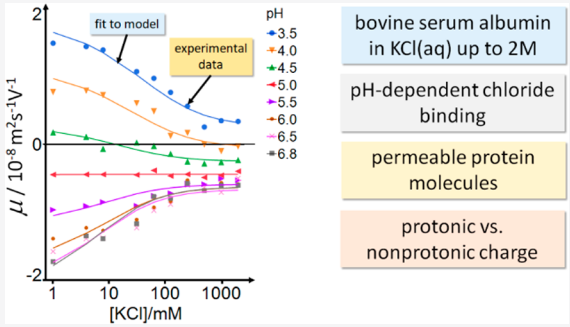

INTRODUCTION

Understanding and controlling the behavior of proteins at, or near, solid−liquid interfaces is of central importance in nanomedicine. In aqueous solutions, such as biofluids, proteins behave as macromolecular lyophilic amphiphiles, exhibiting markedly different behavior toward changes in pH and ionic strength than colloidal dispersions of lyophobic particles or solutions of simple polyelectrolytes. As with other macromolecules, the thermodynamic balance of electrostatic forces, solvation energies, and structural entropy determines the interfacial sorption behavior of proteins. The most common experimental method used to investigate electrical properties is electrophoretic light scattering (ELS), which provides information about the *electrokinetic* properties of the protein−liquid interface. Less commonly used today, though of significant study throughout the twentieth century, is potentiometric titration utilizing a simple acid or base. This yields information about the *electrostatic* properties of the proteins in solution. Whereas potentiometric titration is a straightforward *experimental* procedure, in contrast, ELS is an *instrumental* technique. The ubiquity of commercial ELS instruments in many industries and academic disciplines has led to an unfamiliarity with the principles necessary for correct operation of such devices as well as a proper understanding of the exact theoretical basis for the calculation of the most commonly reported property, the zeta potential.

The primary purpose of this paper is to report a more rigorous methodology to address these issues. It will demonstrate that conventional ELS methodologies have fundamental limitations which prevent the valid use of ELS for the measurement of electrophoretic mobilities of aqueous colloidal systems at ionic strengths near to, or higher than, those typically found in physiological fluids.

Two studies of the measurement of electrophoretic mobilities of bovine serum albumin (BSA) in aqueous potassium chloride solutions as a function of ionic strength and pH are reported. The importance of the nature of electrode material on measurement quality is demonstrated and results compared with data from potentiometric titrations. Further, electrokinetic models are used to predict electrophoretic mobilities from the titration data as a function of ionic strength and pH. It is shown that appropriate selection of an electrokinetic model yields excellent agreement between predicted and experimental electrophoretic mobilities across the ranges of pH and ionic strength studied. The experimental results are explained in terms

Received: June 8, 2020
Revised: June 28, 2020
Published: June 29, 2020

of protonation, chloride counterion binding, and protein molecule porosity. Many of the concepts described herein are well-established in the scientific literature and, therefore, omitted for brevity. Details are provided where they aid understanding of the present work.

Some applications of nanoscience include in vivo administration of aqueous colloidal dispersions.[1,2] Examples of the dispersed materials are sub-100 nm spheroidal lyophobic particles (i.e., lyophobic nanoparticles), such as gold,[3] cesium selenide (quantum dots),[4] and polymer latex particles (e.g., polystyrene).[5] The particles may serve as "carriers" for other components such as proteins that may be physisorbed or chemisorbed at the particle surface. Such a system, therefore, contains both lyophobic and lyophilic colloidal materials. In the case of physisorbed proteins, they exist in dynamic equilibrium between the free solution and adsorbed states.[6] Upon administration to a biofluid, a more complex dynamic equilibrium is established due to the presence of additional proteins and other substances that may compete for adsorption sites at the particle surface. Considerable success was made during the last century to develop and confirm experimentally the necessary theoretical frameworks required to understand the complex sorption behavior of lyophilic macromolecules, including proteins.[6−11]

When a protein adsorbs at a lyophobic particle surface from an aqueous electrolyte solution, the composite particle assumes many of the lyophilic properties of the protein, including the behaviors due to changes in ionic strength and pH.[12−15] Understanding and exploiting this behavior is of central importance to the rapidly emerging concept of the "protein corona" in nanomedicine.[16−24]

Lyophobic (solvent-hating) and lyophilic (solvent-loving) colloids differ in the following important ways.[25−29] Lyophobic colloids (such as dispersions of the preceding examples of carrier particles) are thermodynamically unstable and will undergo irreversible aggregation in the absence of a suitable repulsive force between approaching particles. Lyophilic colloids (such as protein solutions) are thermodynamically stable and will spontaneously form a system with true solution properties. Lyophilic colloids may aggregate but reversibly.

For many lyophobic colloidal systems, aggregation behavior is adequately described by the Derjaguin−Landau−Verwey−Overbeek (DLVO) theory. It is explicitly limited to charged, lyophobic colloidal particles in an aqueous electrolyte solution. The theory further assumes that particle charges and double layer charges are distributed uniformly. Thus, DLVO theory should never be applied to explain or predict the colloidal behavior of proteins in free solution or near solid−liquid interfaces such as those of importance in nanomedicine.

Modern scientific investigation of the effect of electrolytes on proteins dates back to at least the late 17th century, initially focused on understanding the role stomach acid has in digesting proteins.[30] By the mid-1960s, much of the general structure of proteins had been elucidated (such as primary, secondary, and tertiary structures).[31] Proteins comprise amino acid residues joined by peptide bonds with each amino acid residue contributing one carboxylic acid group (−COOH) and one primary amine group ($-NH_2$). The resultant zwitterionic equilibria are

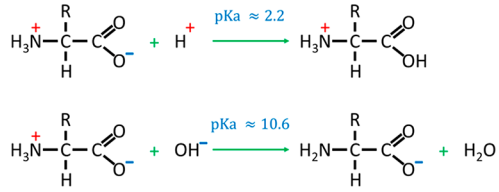

The pK_a values are the averages for the 20 amino acids used in protein synthesis.[32] The values for a particular amino acid depend on the R side group.[33] In a few cases, R is ionizable and introduces a third acid−base equilibrium and, hence, a third pK_a.

At a particular pH, the number of ionized carboxylate groups will exactly equal the number of ionized amino groups. This pH is the isoionic point (iip) and can be determined by the intersection of multiple acid titration curves over a range of ionic strengths.[34,35] The isoelectric point, iep, is defined as the pH at which the velocity of protein molecules in response to an applied electric field is zero. It is an electrokinetic property that indicates the pH at which the net charge of the protein is zero. Thus, if the protein binds with other ions, such as chloride counterions, the net zwitterionic charge will be nonzero at the iep. As a result, iip and iep will not be the same, and their difference will increase with an increasing amount of bound nonprotonic ions, such as counterions adsorbed from the dispersion medium. The iep may be measured using the technique of electrophoresis. The corresponding electrophoretic mobility can be expressed as the sum of a contribution due to protonic charge, μ_H, and a contribution due to counterion charge, μ_{count},

$$\mu = \mu_H + \mu_{count} \tag{1}$$

Electrokinetic Theories. The following treatment of electrophoresis assumes the reader is familiar with the general concepts of the Gouy−Chapman and associated models of the double layer.[25,36] Consideration of electrokinetic theories in this paper is limited to particles possessing sufficiently low electrical charge, and the double layer relaxation effects can be ignored.

A charged particle dispersed in a fluid medium moves with an electrophoretic velocity,v_e, relative to that medium in the presence of an electric field, E. v_e is linearly proportional to E such that

$$v_e = \mu E \tag{2}$$

where the proportionality constant, μ, is the electrophoretic mobility. v_e is the terminal velocity resulting from the balance of the various forces acting on the particle. For the present work, discussion of the practical measurement of μ is limited to ELS. Other experimental methods are described elsewhere.[27,37]

Consider a rigid, spherical particle with an electrical charge, Q, immersed in an electrolyte solution. The particle's radius, a, is defined as the distance from the center of the particle to the plane of shear. The double layer thickness is the reciprocal of the Debye−Hückel parameter, κ,

$$\kappa = \left(\frac{2000F^2I}{\varepsilon_0\varepsilon_r RT}\right)^{1/2} \tag{3}$$

where F is the Faraday constant, ε_0 is the absolute permittivity in vacuo, ε_r is the relative permittivity (dielectric constant) of the fluid, R is the ideal gas constant, T is the absolute temperature, and I is the ionic strength (mol dm^{-3}) given by

$$I = \frac{1}{2}\sum_i c_i z_i^2 \tag{4}$$

https://dx.doi.org/10.1021/acs.langmuir.0c01694
Langmuir XXXX, XXX, XXX−XXX

where c_i and z_i are the molar concentration in bulk solution and valency of ion of type i, respectively.Q must be balanced by the charge of the double layer such that

$$Q = 4\pi\varepsilon_0\varepsilon_r a(1 + \kappa a)\psi_0 \quad (5)$$

where ψ_0 is the potential at the surface of the particle. At a distance r from the center of the particle, the potential, ψ_r, is

$$\psi_r = \psi_0 a\ e^{-\kappa(r-a)}/r \quad (6)$$

At the plane of shear, the potential is defined as the electrokinetic (zeta) potential, ζ. A corresponding electrokinetic charge, Q_e, is

$$Q_e = 4\pi\varepsilon_0\varepsilon_r a(1 + \kappa a)\zeta \quad (7)$$

The product κa is a dimensionless value that indicates the ratio of the particle radius and double layer thickness. Because the plane of shear is the location that delineates the electrophoretic motion of the particle and the stationary bulk fluid, electrophoresis relates to Q_e and ζ not Q or ψ_0.

Two limiting cases exist for relating μ and ζ. The first is for $\kappa a \gg 1$ (i.e., large particles/thin double layers) as given by the Smoluchowski equation,

$$\mu = \frac{\varepsilon_0\varepsilon_r\zeta}{\eta} \quad (8)$$

where η is the viscosity of the fluid. The second is for $\kappa a \ll 1$ (i.e., small particles/thick double layers) as given by the Hückel equation,

$$\mu = \frac{2\varepsilon_0\varepsilon_r\zeta}{3\eta} \quad (9)$$

Henry identified the causes of the discrepancy between eqs 8 and 9 and introduced a correction function, $f_1(\kappa a)$. Hence,

$$\mu = \frac{2\varepsilon_0\varepsilon_r\zeta}{3\eta}\cdot f_1(\kappa a) \quad (10)$$

Substituting eq 7 for ζ in eq 10 gives

$$\mu = \frac{Q_e}{6\pi a(1 + \kappa a)\eta}\cdot f_1(\kappa a) \quad (11)$$

Swan and Furst[38] have approximated $f_1(\kappa a)$ to

$$f_1(\kappa a) = \frac{16 + 18\kappa a + 3(\kappa a)^2}{16 + 18\kappa a + 2(\kappa a)^2} \quad (12)$$

Equation 12 deviates by less than 0.1% from Henry's exact calculation for all κa.

The above relationships between μ, Q_e, and ζ assume nonconducting spherical particles with smooth, impenetrable ("hard") surfaces and do not account for the finite size and hydration of ions at or near the particle surface nor particles that are permeable to the dispersion medium. Thus, although they may be reasonably valid for the types of carrier particles mentioned above, critically they are not appropriate for protein molecules in free solution or adsorbed onto carrier particles.

The conformation of globular proteins in aqueous solution resembles a core of densely packed hydrophobic amino acid side chains surrounded by a less densely packed shell of hydrophilic amino acid side chains. The core is likely to carry little electrical charge, whereas the shell will possess charge according to the zwitterionic equilibria described earlier and any bound nonprotonic ions.[39−41] Such charges are spatially fixed and nominally evenly distributed. Unlike the hydrophobic core, the hydrophilic shell is permeable to the surrounding liquid. Bound ions such as chloride are likely to be located within the protein structure as a result of coordination between the ions and multiple amino acid residues.[42] The number of bound ions may depend on the pH and ionic strength of the solution. For example, Scatchard et al.[43] found that the number of chloride ions bound to one molecule of bovine serum mercaptalbumin in 10 mM aqueous sodium chloride solution was approximately 2 at pH 5.5, increasing to approximately 13 at pH 3.5. The overall structure of a globular protein in aqueous solution resembles a "soft" particle,[44] with protonic charges at the exterior surface and nonprotonic charges within the interior of the molecule. (The terms "hard" and "soft" used herein are those used in the traditional colloid science literature and should not be confused with the same terms used when describing the protein corona.)

There are two limiting cases of a soft sphere. In the case of a shell of zero thickness, the particle is the same as a rigid, hard sphere. A particle with a core diameter of zero behaves as a solvated polymer molecule and, more specifically, a polyelectrolyte in the instance of a charged particle. Several theoretical treatments of the electrophoretic behavior of polyelectrolytes (including proteins) have been reported.[44−53] Most of these require numerical analysis or semianalytical computation and, therefore, are of limited practical application. The theories of the electrophoresis of rigid spheres and, separately, spherical polyelectrolytes often are considered mutually inconsistent. Ohshima has developed an analytical electrokinetic model for the electrophoretic mobility of soft particles that is consistent with both theoretical frameworks.[44] However, the approximate electrophoretic mobility model reported by Ohshima is limited to $\kappa a \gg 1$ and, therefore, cannot be applied to proteins in free solution at physiological ionic strengths. The Hermans−Fujita model[54] considers the flow of liquid through a porous sphere. In the case of a polymer molecule, the liquid flow is determined by the forces arising from the interaction between the liquid and the polymer chain segments when the polymer molecule is moving in response to an external field. In the case of a gravitational field, the polymer motion is sedimentation. For an external electric field, the motion is electrophoresis of a polyelectrolyte. The Hermans−Fujita equation for μ can be written as[48]

$$\mu = \frac{\rho}{\nu f}\left[1 + \frac{\Phi(\sigma, \beta)}{1 - \tanh(\sigma)/\sigma}\right] \quad (13)$$

where

$$\Phi(\sigma, \beta) = \frac{2}{3}(\sigma^2/\beta^2)\ e^{-\beta}\cosh\beta\{(1 - \tanh(\beta)/\beta) \times (1 + \beta\tanh(\sigma)/\sigma) + [\beta^2(1 + \beta)/(\beta^2 - \sigma^2)] \times (\tanh(\beta)/\beta - \tanh(\sigma)/\sigma)\} \quad (14)$$

with

$$\beta = \kappa a \quad (15)$$

and

$$\sigma^2 = \nu f a^2/\eta \quad (16)$$

σ is the Debye−Bueche shielding ratio,[55] a is the radius of the polyelectrolyte containing N segments, ρ is the number density

https://dx.doi.org/10.1021/acs.langmuir.0c01694
Langmuir XXXX, XXX, XXX−XXX

of spatially fixed charges on the polyelectrolyte, and ν is the segment density such that

$$N = \frac{4}{3}\pi a^3 \nu \tag{17}$$

σ represents the distortion of linear flow of liquid through the polymer due to the presence of electrically charged segments and f is a frictional factor for the liquid flowing through the polymer molecule. For liquid flow through the molecule with no friction (i.e., free draining liquid), $\sigma = 0$. For an impermeable molecule, the friction is infinitely high and $\sigma = \infty$. An additional quantity, λ, is defined by[55]

$$\lambda^2 = \frac{2}{3}\nu f/\eta \tag{18}$$

which, in effect, scales the shielding ratio with respect to the molecular cross-sectional area. Ohshima interprets $1/\lambda$ as "the distance between the slipping plane and the bulk phase of the surface layer" and "that a small shift of the slipping plane causes no effects on the mobility value. Therefore, the mobility of soft particles is insensitive to the position of the slipping plane and the zeta potential loses its meaning".[44]

Hermans[49] introduced an approximation to the Hermans–Fujita model such that

$$\mu = \frac{\rho}{\nu f}\left\{1 - \frac{\alpha^2}{\beta} e^{-\beta} \cosh\beta(1 - \tanh(\beta)/\beta) + \frac{(1+\beta)\alpha^2}{\beta^2 - \alpha^2} e^{-\beta} \cosh\beta\left[1 - \frac{\alpha^2}{\beta^2}\frac{(1 - \tanh(\beta)/\beta)}{(1 - \tanh(\alpha)/\alpha)}\right]\right\} \tag{19}$$

where

$$\alpha = \lambda a \tag{20}$$

There are two important limiting cases for μ given by eq 19, for a free draining porous particle and for a nonfree draining porous particle.

In the first case, $\alpha = 0$. Thus, eq 19 reduces to

$$\mu = \frac{\rho}{\nu f} \tag{21}$$

i.e., the electrophoretic mobility for a free draining porous particle containing spatially fixed charges is constant for all electrolyte concentrations.

In the second case, when the bulk electrolyte concentration is infinitely high, then $\beta = \infty$ and, in the limit, eq 19 also becomes

$$\mu = \frac{\rho}{\nu f} \tag{22}$$

In this instance, the electrophoretic mobility for a nonfree draining porous particle containing spatially fixed charges now limits to a constant value with increasing electrolyte concentration. This is unlike the case for a rigid impermeable spherical particle for which the electrophoretic mobility is predicted to limit to zero with increasing electrolyte concentration (eq 11).

Using eq 18, both eqs 21 and 22 can be expressed as

$$\mu = \frac{2\rho}{3\eta\lambda^2} \tag{23}$$

In principle, determination of the electrophoretic mobility as a function of electrolyte concentration should indicate whether the particles exhibit rigid or porous behavior. This requires measurements to be made at nominally $\kappa a > 10$. For protein molecules in free solution, this corresponds to ionic strengths greater than nominally 500 mM. Hence, to select the most appropriate electrokinetic model, experimental data may need to be collected at ionic strengths up to as high as 2 M.

Under physiological conditions, the concentration of proteins in solution is sufficiently high that the mean intermolecular distance is comparable to the double layer thickness, leading to "overlap" of the double layers of neighboring protein molecules. This may result in a lower electrophoretic mobility than the nonoverlapped (dilute) case for a given κa. Ohshima has reported a general analytical expression for the electrophoretic mobility of identical rigid spherical particles in concentrated dispersions,[56]

$$\mu = \frac{2\varepsilon_0\varepsilon_r\zeta}{3\eta} \cdot f(\kappa a, \phi) \tag{24}$$

where

$$f(\kappa a, \phi) = \left\{1 + \frac{1}{2(1 + \delta/(\kappa a))^3}\right\} M_1(\kappa a, \phi) + M_2(\kappa a, \phi) \tag{25}$$

and

$$M_1(\kappa a, \phi) = 1 - \frac{3}{(\kappa a)^2}\frac{\phi}{1-\phi}(1 + \kappa a R) + \frac{(\kappa a)^2}{5P}\frac{1}{\phi^{2/3}}\left(1 + \frac{1-\phi}{3} - \frac{3}{1-\phi} + \frac{3\phi^{1/3}}{1-\phi}\right) \tag{26}$$

$$M_2(\kappa a, \phi) = \frac{2(\kappa a)^2}{9P}\frac{1 + \phi/2}{1-\phi}\left(\phi^{1/3} + \frac{1}{\phi^{2/3}} - \frac{9}{5\phi^{1/3}} - \frac{\phi^{4/3}}{5}\right) \tag{27}$$

$$P = \cosh[\kappa a(\phi^{-1/3} - 1)] - \frac{\phi^{1/3}}{\kappa a}\sinh[\kappa a(\phi^{-1/3} - 1)] \tag{28}$$

$$R = \frac{1 - \kappa a\phi^{-1/3}\tanh[\kappa a(\phi^{-1/3} - 1)]}{\tanh[\kappa a(\phi^{-1/3} - 1)] - \kappa a\phi^{-1/3}} \tag{29}$$

with δ chosen to be

$$\delta = \frac{2.5}{1 + 2e^{-\kappa a}} \tag{30}$$

At $\phi = 0$, $f(\kappa a,\phi)$ is equal to Henry's function, $f_1(\kappa a)$, defined in eq 11.

For albumin proteins in physiological fluids, $\phi \sim 0.05$ and $f(\kappa a,\phi)$ deviates significantly from $f_1(\kappa a)$ for κa below ~1. This corresponds to ionic strengths less than nominally 10 mM. Hence, to select the most appropriate electrokinetic model, experimental data should be collected at ionic strengths down to 1 mM.

https://dx.doi.org/10.1021/acs.langmuir.0c01694
Langmuir XXXX, XXX, XXX−XXX

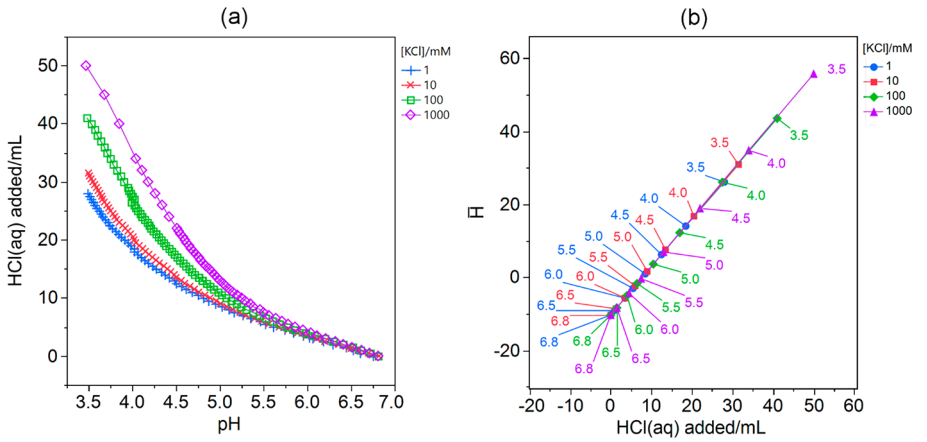

Figure 1. (a) Raw titration data showing the volume of titrant added vs pH. Data are not compensated for dilution by added titrant or apparent hydrogen activity coefficients. (b) Net protonic charge per protein molecule ($\bar{H}$) vs the amount of titrant added. Data are compensated for dilution by added titrant and apparent hydrogen activity coefficients. Numeric datum labels indicate the pHs at which electrophoretic mobility measurements were performed.

For a protein in aqueous electrolyte solution, Q can be expressed as the sum of a contribution due to protonic charge, Q_H, and a contribution due to counterion charge, Q_{count},

$$Q = Q_H + Q_{count} \tag{31}$$

The most appropriate electrokinetic model should be able to identify double layer overlap, the presence of nonprotonic charge, the softness of the protein molecules, and the iip. Further, the model should be consistent with protonic charge that is insensitive to ionic strength. Thus, both potentiometric and electrokinetic data must be obtained experimentally at a range of pHs and ionic strengths.

EXPERIMENTAL SECTION

Materials. BSA (lyophilized heat shock fraction V, >98% purity, biotechnology grade) was purchased from Biomatik Corporation (Cambridge, Ontario). Platinum and palladium sheets were purchased from Hauser and Miller (St. Louis, MO). Lead(II) acetate trihydrate and hydrogen hexachloroplatinate (IV) hydrate were purchased from Thermo Fisher Scientific Inc. (Waltham, MA). All materials were used as received.

Solution Preparation. A total of 5.0 g of BSA was dissolved in 100 mL of aqueous KCl solution for each KCl concentration studied. Titrant solutions of 0.10 M HCl(aq) were prepared at the same KCl concentration as the analytes. Platinizing solution was prepared by dissolving 1 g of hydrogen hexachloroplatinate(IV) hydrate in 100 mL 0.015 w/v (%) aqueous lead(II) acetate trihydrate solution.

Study 1. The first study was performed on BSA solutions at KCl concentrations of 0.001, 0.01, 0.1, and 1 M. Potentiometric titrations were conducted for each solution according to the method described below. For each solution, electrophoretic mobilities were measured at their equilibrium pH values (i.e., the pH of the solution without the addition of HCl(aq)) and nominal pHs of 6.5, 6.0, 5.5, 5.0, 4.5, 4.0, and 3.5. Electrophoretic mobilities at each KCl concentration and pH were determined using, separately, platinum, platinum black,[57] and palladium electrodes. Additional investigations were made of the effects of electrode material on the electrolysis of KCl solutions in the presence and absence of BSA. Scanning electron microscopy (SEM) and energy dispersive spectrometry (EDS) analyses were performed using a Quanta 200 xTm scanning electron microscope (Thermo Fisher Scientific Inc., Waltham, MA) with a QUANTAX EDS (Bruker Corporation, Billerica, MA).

Study 2. The second study was performed on BSA solutions at nine KCl concentrations in the range from 1 mM to 2 M. Potentiometric titrations were not conducted. For each solution, electrophoretic mobilities were measured at their equilibrium pH values (i.e., the pH of the solution without the addition of HCl(aq)) and nominal pHs of 6.5, 6.0, 5.5, 5.0, 4.5, 4.0, and 3.5. Electrophoretic mobilities at each KCl concentration and pH were determined using platinum black electrodes only.

Potentiometric Titration. Potentiometric titration was performed manually. A volume of 100 mL of analyte solution was prepared in a 250 mL glass bottle. The solution was stirred with a magnetic follower. Titrant solution was put in a volumetric 50 mL buret, and a standard glass pH electrode was immersed in the analyte solution. The general procedure of Sørensen et al.[34] was followed to estimate the net protonic charge per protein molecule. For a given KCl concentration, the corresponding BSA solution was titrated first. Titrant was added in 0.5 mL aliquots, and the pH was recorded. It was observed that sufficient equilibration of the pH occurred within 30 s of the addition of titrant. The titration was continued until a solution pH of 3.5 was obtained. A "blank" titration was performed for an aqueous solution of KCl at the same concentration as the BSA solution. The total volume of titrant added was the same as used for the BSA solution. The data for the blank titration were used to determine the apparent hydrogen activity coefficient in order to compensate for the KCl concentration dependency of both the hydrogen activity in bulk solution and the galvanic response of the glass electrode. All measurements were performed at 25 ± 1 °C.

Electrophoretic Mobility Measurement. Electrophoretic mobilities were determined using an ELS apparatus functionally equivalent to the first ELS instrument to employ the phase analysis light scattering (PALS) data analysis method and which employed a crossed-beam optical configuration (in contrast to the more common reference beam configuration used in current commercial ELS instruments), together with the more traditional laser Doppler electrophoresis (LDE) methodology.[58,59]

The electrode assembly used was a variation of that described by Uzgiris.[60] Disposable polystyrene semimicro-cuvettes (4 mm path length) were used as the sample holders. Two identical parallel plate electrodes, 4 mm apart, were used to provide the driving voltage across the sample. The volume of the sample required for measurement was approximately 0.25 mL. BSA solutions for analysis were measured without further dilution. The samples were filtered through 0.2 μm poly(ether sulfone) syringe filters directly into the sample holders. The sample temperature was measured with a miniature NTC-type thermistor that was placed in direct contact with the sample. It was positioned at the midpoint between the electrodes and approximately 2 mm above the intersection point of the two laser beams. Temperature control was achieved by placing the sample cuvette in an aluminum block that acted as a heat transfer device between it and cooled water circulated through channels within the block. The required temperature

https://dx.doi.org/10.1021/acs.langmuir.0c01694
Langmuir XXXX, XXX, XXX−XXX

of the water was dependent on the amount of Joule heating of the sample and, therefore, the conductivity of the sample and the magnitude of the voltage applied across the electrodes. Complex impedance analysis of the electrode waveform was used to quantify electrode polarization and Joule heating. It was also used to qualitatively identify electrolysis. Mobility measurements were made using sinusoidal and, separately, square electrode signal waveforms with typical amplitudes of 6 to 10 V (most commonly 8 V) and typical frequencies of 2 to 64 Hz (most commonly 64 Hz). The scattered light data were analyzed using both the PALS and the LDE methods simultaneously, i.e., the same scattered light data were used to calculate the electrophoretic mobility using each data analysis method. Data were collected for 30−60 s. For each sample, typically 8 to 12 independent measurements were made according to the combination of waveform characteristics required. A description of the differences between the original PALS instrument and the instrument used for this work is provided elsewhere.[61]

RESULTS AND DISCUSSION

Study 1. *Potentiometric Titration.* Figure 1a shows the titration data obtained for each of the BSA solutions. The data are plotted as the volume of titrant added as a function of solution pH. The data have not been corrected for dilution effects or apparent hydrogen activity coefficients.[34] Hence, the amount of titrant required to achieve a specific solution pH increases with increasing [KCl]. Following the required correction for these two phenomena, the apparent net number of protonic charges per protein molecule, $\bar{H}$, can be calculated. Figure 1b shows $\bar{H}$ plotted as a function of the volume of added titrant. The superposition of linear responses for each [KCl] indicates that the net protein charge is now, as expected, independent of [KCl]. This illustrates the importance of the two corrections. The numeric datum labels indicate the pHs at which electrophoretic mobility measurements were performed.

Figure 2 shows $\bar{H}$ plotted as a function of [KCl] at the pH values used for electrophoretic mobility measurements. The

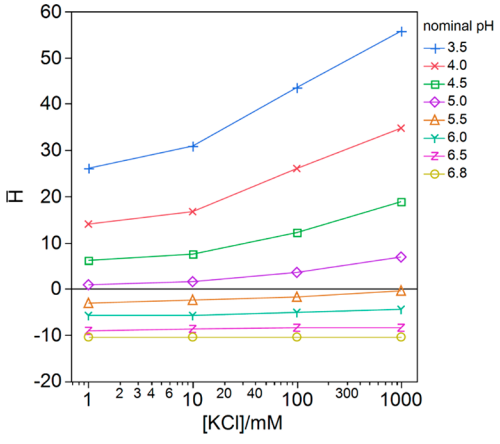

Figure 2. Net protonic charge per protein molecule ($\bar{H}$) vs [KCl] at the nominal pH values at which electrophoretic mobility measurements were performed.

increase in $\bar{H}$ with increasing [KCl] illustrates the decrease in the hydrogen activity coefficient at higher [KCl]. Previous researchers have not accounted for this and so have erroneously concluded that the net protonic charge is dependent on the concentration of the electrolyte.[62] Given that the net protonic charge is independent of [KCl], the $\bar{H}$ data at a given pH can be extrapolated to zero [KCl] in order to obtain a more faithful estimate of the net protonic charge, $\bar{H}_0$. These values are used as the net protonic charge per molecule required by Study 2 for the electrokinetic modeling of the experimental electrophoretic mobility data.

Electrophoretic Mobility. Figure 3a−f show the mean values of the corresponding individual PALS and LDE electrophoretic mobility data. The vertical bars for each datum point indicate the range of the individual measurements used to calculate the mean value. The electrophoretic mobility data are presented as a function of pH (Figure 3a−c) and as a function of [KCl] (Figure 3d−f) for each electrode material separately. The data in Figure 3a−c are grouped by [KCl], whereas the data in Figure 3d−f are grouped by pH.

The most significant observation is that the experimental electrophoretic mobilities vary according to the choice of the electrode material. The results obtained using Pt black electrodes demonstrate the expected dependencies on pH and [KCl] as reported by other researchers. The mobility−pH curves are well-defined at each [KCl]. As expected, the choice of electrode material has negligible effects on the measurements at 1 mM [KCl]. At 10 mM [KCl], there is evidence that the magnitudes of the electrophoretic mobility data obtained using Pd electrodes are lower than for Pt and Pt black electrodes. Data obtained using Pt electrodes are in excellent agreement with those obtained with Pt black electrodes. At 100 mM [KCl], data obtained with Pd electrodes show significant deviation from those obtained with Pt and Pt black electrodes, notably below pH 5.0. At 1000 mM [KCl], both Pd and Pt electrodes yield data significantly different from those obtained with Pt black electrodes. Neither Pd nor Pt electrodes permit confident measurement of electrophoretic mobility at 1000 mM [KCl]. Poor measurements are obtained with Pd electrodes at 100 mM [KCl] and higher. The more popular of the current generation of commercial ELS instruments now use Pd Uzgiris-type electrode assemblies. (Although some manufacturers offer Au electrodes, they are not considered for this work. The present author previously observed (unpublished) that Au electrodes demonstrate similar behavior to Pt electrodes together with significant "pitting" of the electrode surfaces because of electrolysis.) Measurements made with those instruments at physiological ionic strengths and higher will, therefore, be subject to significant uncertainty and, accordingly, any scientific conclusions drawn from such measurements must be treated with caution. The use of Pt black electrodes with commercial instruments is readily achievable and would significantly reduce this risk.

Figure 3a−c clearly illustrates the inferior performance of Pt and Pd electrodes compared to Pt black electrodes. The electrophoretic mobility data obtained using Pt black electrodes show a well-defined common intersection point for each [KCl] data set (approximately -4×10^{-9} m^2 s^{-1} V^{-1} between pH 4.5 and 5.0). By analogy with acid titration, this indicates that the net electrokinetic charge per protein molecule is independent of [KCl] and that the protein possesses nonprotonic negative charge in addition to the protonic charge measured by the acid titration. This common intersection point is the isoionic point. The data obtained with both the Pt and Pd electrodes fail to identify a common intersection point. Thus, the use of Pt or Pd electrodes is not recommended. The data shown in Figure 3d−f further emphasize the inappropriate use of Pt or Pd electrodes. The data obtained with Pt black electrodes suggest that the electrophoretic mobility at each pH will converge to the isoionic point at [KCl] above 1000 mM. However, as will be seen below

https://dx.doi.org/10.1021/acs.langmuir.0c01694
Langmuir XXXX, XXX, XXX−XXX

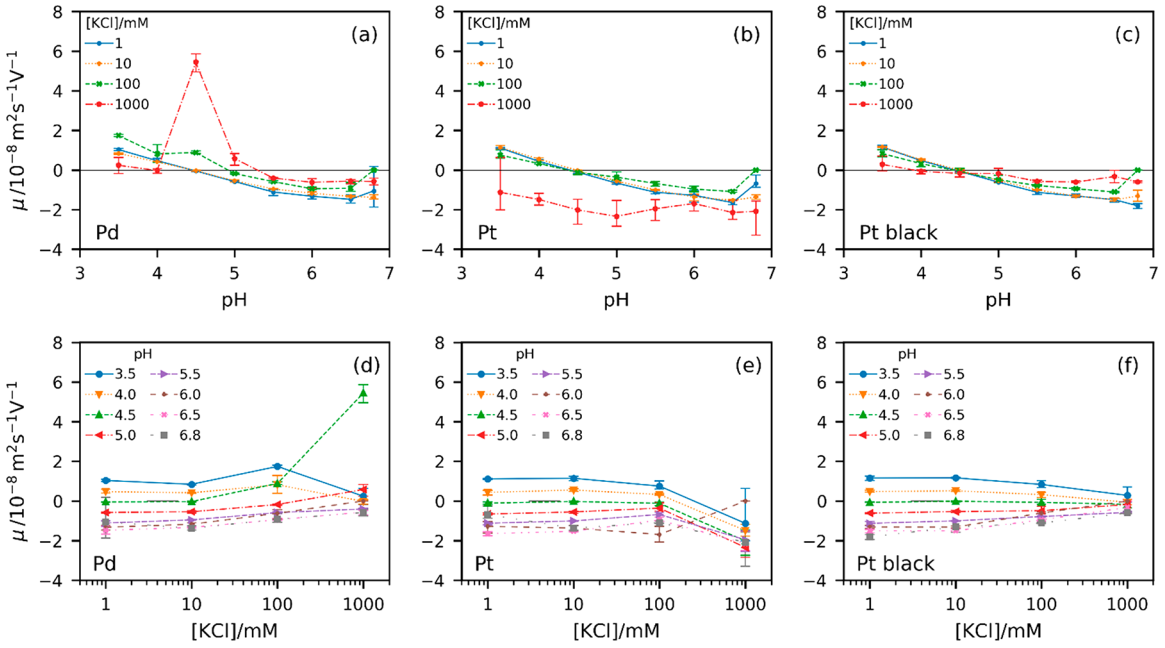

Figure 3. Mean values of the corresponding individual PALS and LDE electrophoretic mobility data. Vertical bars for each datum point indicate the range of the individual measurements used to calculate the mean value. Data are grouped in columns according to the electrode material (left, middle, and right columns for Pd, Pt, and Pt black, respectively). The top row (a–c) shows electrophoretic mobility data plotted as a function of pH for each [KCl] separately. The bottom row (d–f) shows electrophoretic mobility data plotted as a function of [KCl] for each pH separately. All measurements made using an applied voltage of 8 V at 64 Hz using both square and sinusoidal waveforms.

in Study 2, the data will show that the electrophoretic mobility reaches a pH-dependent constant value above 1000 mM.

In support of the measurement data, visual assessment of the appearance of the electrodes before and after application of the electric field indicates that electrolysis is the primary cause of the poor performance of Pt and Pd electrodes. Figure 4 shows the

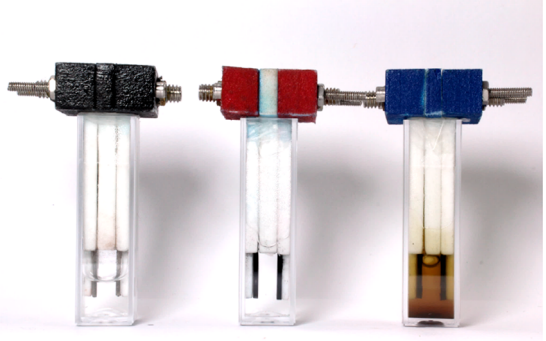

Figure 4. Appearance of 100 mM KCl(aq) solution after exposure to an 8 V/8 Hz square waveform for 5 min using Pt (left/black), Pt black (center/red), and Pd (right/blue) electrodes.

appearance of 100 mM KCl(aq) solution (filtered through 0.2 μm poly(ether sulfone) syringe filters) after exposure to an 8 V/8 Hz square waveform for 5 min using Pt (left/black), Pt black (center/red), and Pd (right/blue) electrodes.

A large gas bubble is evident in the Pt case that is chlorine formed by electrolysis at the electrode–electrolyte interface. No visible changes were observed when Pt black electrodes were used. Significant discoloration of the electrolyte solution and the electrodes occurred when Pd was used as the electrode material.

A pure solution of a simple electrolyte should not scatter light from a laser source directed through the solution. Any scattering from an electrolyte solution after the application of an electric field will indicate the formation of colloidal debris from degradation because of electrolysis. The formation of such contaminants during the measurement of a colloidal sample may adversely affect the validity of the experimental results. The reasons for this include significant contribution by the contaminating particles to the scattered light intensity and aggregation of the contaminating particles with the particles intended for measurement. Such formation was assessed for filtered 10 mM KCl(aq) solutions following application an electric field for 30 min (8 V/8 Hz square waveform). Figure 5a shows the amount of light scattered from a laser beam passing through the solutions following the removal of the electrodes.

The photographs were taken at a scattering angle of approximately 90 deg. The control sample was filtered 10 mM KCl(aq) that had not been in contact with any surfaces except those of the cuvette. There is no evidence for particle formation due to the use of Pt black electrodes. However, the use of Pt or Pd electrodes leads to the formation of colloidal particles. In the case of Pd electrodes, the scattering intensity is comparable to or greater than that typically observed for uncontaminated colloidal samples. The appearance before removal of the electrode assembly of the solution subjected to the electric field using Pd electrodes is shown in Figure 5b. Figure 5c shows the appearance of the surface of the Pd electrode after application of the electric field. The dark surfaces are those that were in contact with the solution, whereas the shiny surfaces were not.

In the presence of protein, the use of Pd electrodes did not result in the discoloration of the sample, but the portion of the electrode material in contact with the sample became black, as with the electrolyte-only case. Optical imaging (Figure 6a) and SEM imaging (Figure 6b) indicate that a thin film formed at the electrode–liquid interface.

https://dx.doi.org/10.1021/acs.langmuir.0c01694
Langmuir XXXX, XXX, XXX–XXX

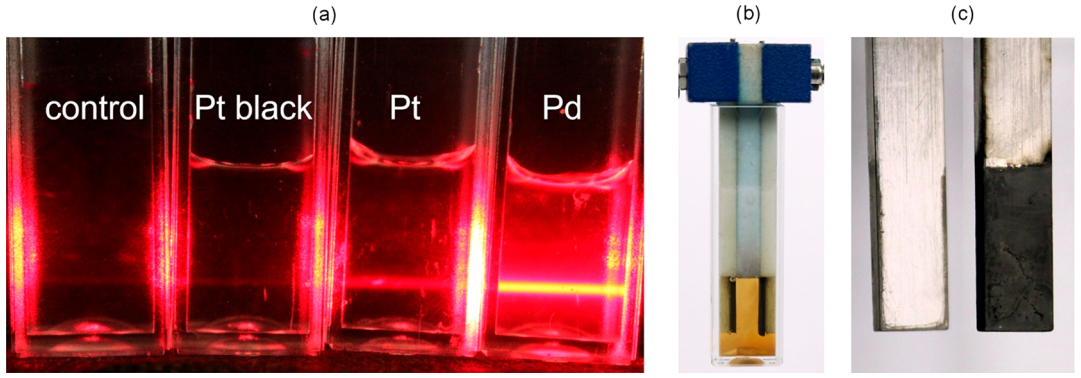

Figure 5. Effect of applying an 8 V/8 Hz square waveform to 10 mM KCl(aq) solution for 30 min. (a) Appearance of laser light scattered by solution following removal of the electrodes (rightmost three samples) and a control solution not exposed to an electric field (leftmost sample); (b) appearance before removal of the electrode assembly of the solution subjected to the electric field using Pd electrodes; and (c) appearance of the surface of a Pd electrode after application of the electric field. The dark surfaces are those that were in contact with the solution, whereas the shiny surfaces were not.

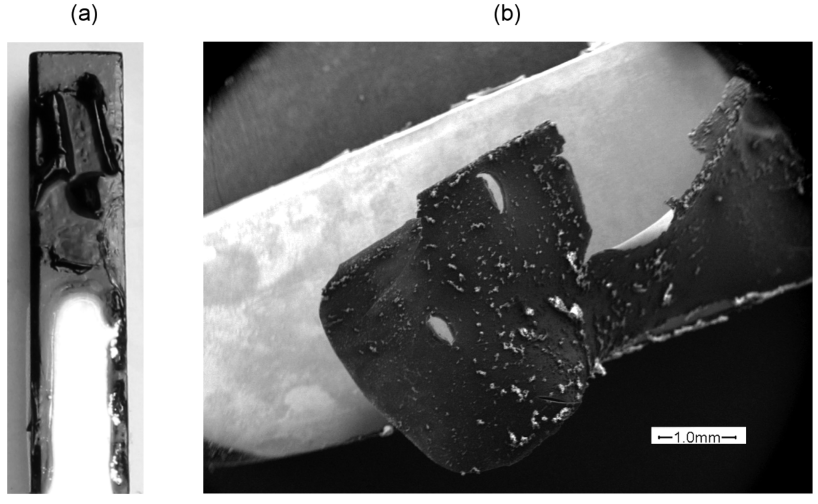

Figure 6. (a) Optical imaging and (b) SEM imaging of a Pd electrode removed from a solution of BSA in 100 mM KCl(aq) after application of an 8 V/8 Hz square waveform for 5 min.

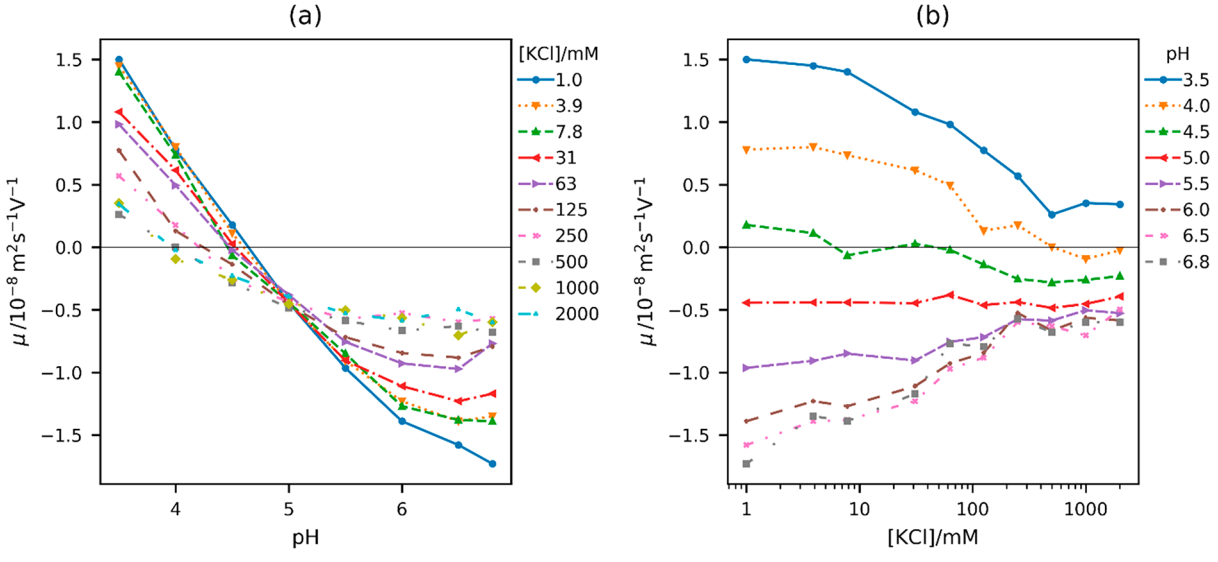

Figure 7. (a) Experimental electrophoretic mobilities for the BSA solutions grouped by [KCl] and plotted as a function of pH. (b) Same data grouped by pH and plotted as a function of [KCl]. The lines are visual guides only.

The optical image shows that the film is black and partially detached from the electrode surface. The SEM image suggests that the film is a thin, electrically insulating layer of material that readily detaches from the surface of the electrode. The latter is

https://dx.doi.org/10.1021/acs.langmuir.0c01694
Langmuir XXXX, XXX, XXX−XXX

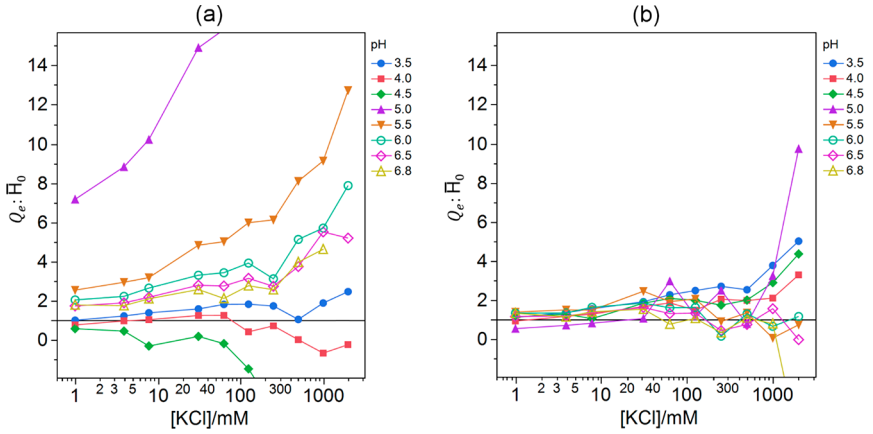

Figure 8. Ratio of net electrokinetic charge per molecule calculated from experimental electrophoretic mobility data to the net protonic charge per molecule measured by titration, calculated using the Henry model (a) without and (b) with the counterion contribution to electrophoretic mobility.

exposed in a near-pristine state. EDS analysis of the detached layer confirms that it is primarily proteinaceous with approximately 0.5% Pd by the number of atoms. The C/N ratio of the detached layer (64:36% by number of atoms) was found to be the same as for protein recovered from KCl(aq) solution that had not been exposed to an electric field.

In the presence of protein, the use of Pt electrodes did not result in the formation of chlorine bubbles in the bulk sample. Instead (not shown), a transparent, colorless film formed at the electrode−liquid interface. The film appeared to have bubbles trapped within itself. No discoloration of the Pt occurred. A common unsubstantiated assertion by manufacturers and users of the current generation of ELS instruments is that the darkening of electrodes following measurement of protein-containing samples is due to chemical degradation of the protein, euphemistically referred to as "cooking" the protein.[63−65] The observations reported herein indicate that such behavior does not occur. As stated earlier, Pd is the most common electrode material used in commercial ELS instruments. The results of this study demonstrate that Pd should not be used for the measurement of electrophoretic mobility of samples with ionic strengths of the order of 10 mM or higher. The interpretation of data obtained using Pd electrodes and reported in the scientific literature must be considered with caution. The results also speak to the need for visual observation and cleaning of electrodes after any measurement as good operational practice.

Study 2. *Experimental Electrophoretic Mobility Data.* Figure 7a shows the experimental electrophoretic mobilities for the BSA solutions grouped by [KCl] and plotted as a function of pH. Figure 7b shows the same data grouped by pH and plotted as a function of [KCl].

Each datum point is the mean of typically 8 to 16 individual 30-s measurements using an applied electrode voltage of nominally 8 V at 16 Hz and, separately, 64 Hz. Half of the measurements were performed with a square electric field waveform, and the other half used a sinusoidal electric field waveform. As with Study 1, electrophoretic mobilities were calculated using both the PALS and LDE data analysis methods. Range bars are excluded for clarity. The data confirm the main observations of Study 1. Figure 7a shows the presence of a well-defined common intersection point of the electrophoretic mobility vs pH responses for each [KCl] (approximately -4×10^{-9} m^2 s^{-1} V^{-1} near pH 5.0). For each pH studied, the electrophoretic mobility decreases with increasing [KCl] and reaches a pH-dependent limiting value above approximately 500 mM [KCl]. Similarly, the electrophoretic mobility approaches a pH-dependent limiting value below approximately 10 mM [KCl].

As discussed in the Introduction, many electrokinetic models exist that relate particle net charge to electrophoretic mobility. However, the validity of a given model depends critically on whether the sample being studied meets the assumptions of the model. For example, the Hückel, Smoluchowski, and Henry models assume impermeable smooth spheres with uniformly distributed surface charge. Therefore, it is unlikely that those models will apply to proteins. The experimental electrophoretic mobility data obtained for Study 2 provide a high-quality set of data, covering a wide range of pH values and electrolyte concentrations, that can be used to compare the prediction of electrophoretic mobility from the titration data by various electrokinetic models. To be of practical benefit, electrokinetic models should be analytical and not require computationally intensive numerical analysis, nor parameters that cannot be realistically specified. A valid model must predict four key features of the experimental data set, namely, the pH-dependent limiting value at [KCl] < 10 mM, the pH-dependent limiting value at [KCl] > 500 mM, the presence of an isoionic point, and nonzero electrophoretic mobility at the isoionic point.

Henry Model. Many modern commercial ELS instruments estimate zeta potential from experimental electrophoretic mobility measurements using either the Hückel model, eq 9, or the Smoluchowski model, eq 8, with some instruments able to use the more general Henry model, eq 10. It is uncommon for commercial instruments to estimate the electrokinetic charge, Q_e, by using, for example, the corresponding Henry equation, eq 11. Assessment of the validity of the Henry model can be made by comparing the estimates of Q_e from the experimental electrophoretic mobility data with the experimental net protonic charge per protein, $\bar{H}_0$, obtained from potentiometric titration. The ratio $Q_e/\bar{H}_0$ should equal unity if the Henry model is valid. Figure 8a shows the calculated $Q_e/\bar{H}_0$ values for the experimental electrophoretic mobility data (Figure 7).

Good agreement between the Henry model and the experimental data is only obtained at nominally pH ≤ 4.0 and nominally [KCl] ≤ 100 mM. The general lack of agreement at the other conditions is, in part, a result of neglecting the contribution to the electrophoretic mobility of bound counterions, μ_{count}. According to eq 1, $\mu_{exp} = \mu_H + \mu_{count}$, where μ_{count} is the value of μ_{exp} at the isoionic point identified in Figure 7a.

https://dx.doi.org/10.1021/acs.langmuir.0c01694
Langmuir XXXX, XXX, XXX−XXX

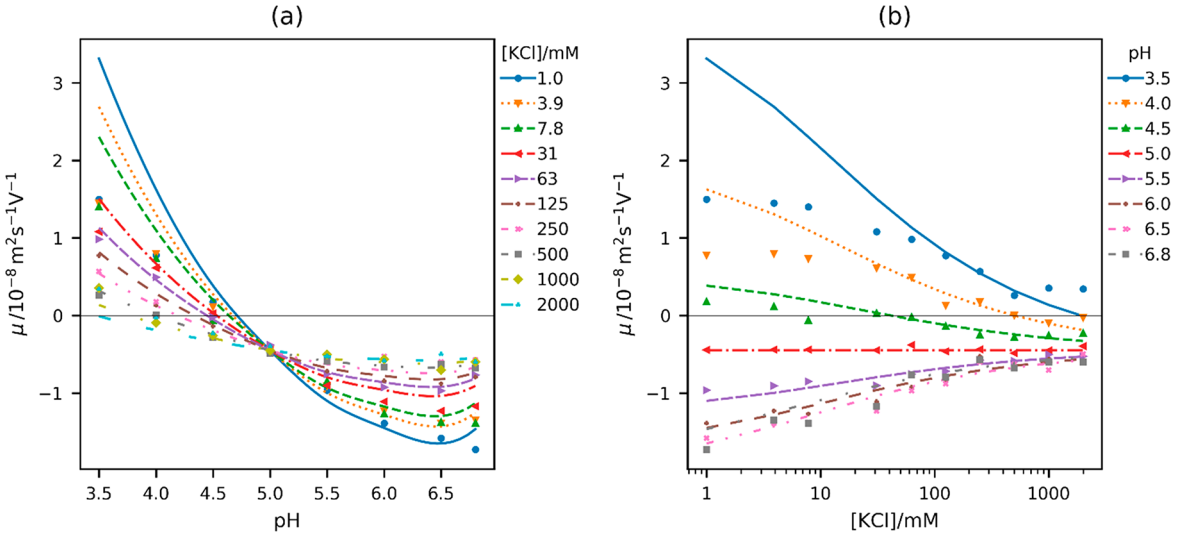

Figure 9. Electrophoretic mobility (a) as a function of pH (grouped by [KCl]) and (b) as a function of [KCl] (grouped by pH). Datum markers are experimental data. Lines show the fit to the Henry model (eq 11).

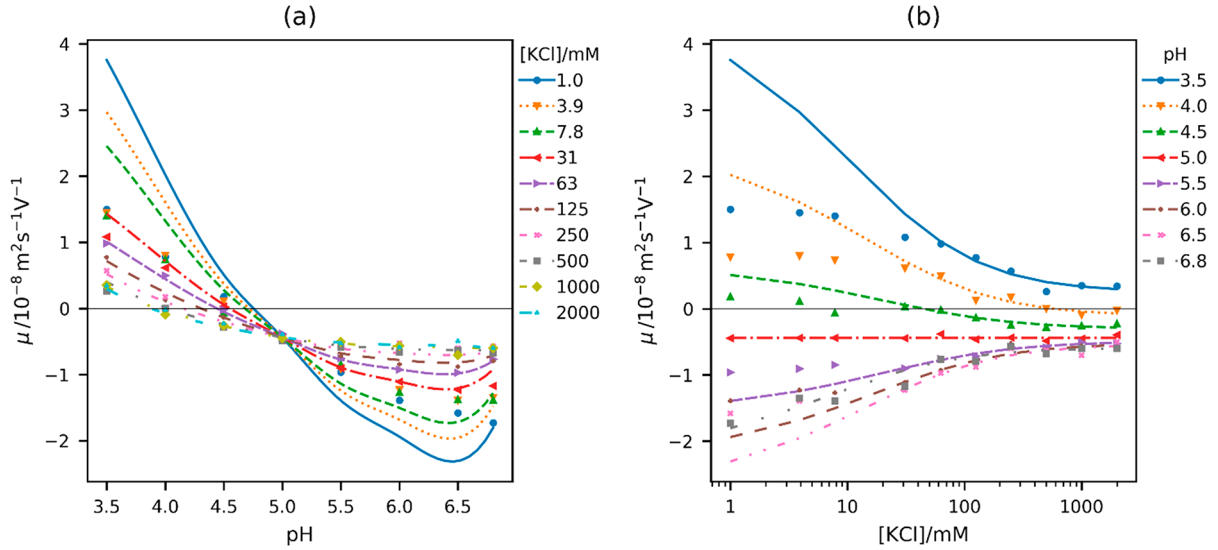

Figure 10. Electrophoretic mobility (a) as a function of pH (grouped by [KCl]) and (b) as a function of [KCl] (grouped by pH). Datum markers are experimental data. Lines show the fit to the Hermans model (eq 19).

Figure 8b shows the calculated $Q_e/\bar{H}_0$ values using μ_H instead of μ_{exp}. There is better agreement between the theoretical values and the experimental data, notably for [KCl] ≤ 10 mM at all pHs. However, significant deviations from the expected value occur above 100 mM [KCl], particularly for pH ≤ 5.0. The contribution of nonprotonic charge to the electrokinetic charge can only be obtained by measuring the electrophoretic mobility of the particles of interest at multiple pH values and electrolyte concentrations. In practice, this is seldom done. Instead, measurements are made at a single pH-electrolyte concentration combination. Less often, measurements are made at a fixed pH and multiple electrolyte concentrations or a fixed electrolyte concentration and multiple pH values. Unless there is a supporting argument that the particles being measured possess only protonic charge, then the conclusions drawn from the estimated electrokinetic charge (or potential) will have a high likelihood of being invalid.

The preceding validation of the Henry model used the experimental electrophoretic mobility data to estimate the electrokinetic charge and compare it to the protonic charge obtain by titration. The validity of the Henry model can also be assessed by comparing the experimental electrophoretic mobilities with those calculated from the experimental protonic charge obtained by titration. Figure 9 shows the comparison between the experimental electrophoretic mobility data (datum markers) and the predicted electrophoretic mobility (lines).

Nonlinear least-squares analysis was used to estimate the values of a at each pH according to eq 11. Only data for [KCl] > 100 mM were used. The electrophoretic mobility at the iip was subtracted from each datum point prior to analysis and added to the predicted values. This allows the modeling procedure to account for the nonzero electrophoretic mobility at the iip (i.e., likely due to counterion binding). This is only possible if experimental data were obtained as a function of pH and [KCl]. Although there is qualitative agreement between the experimental data and predicted electrophoretic mobility as far as general trends are concerned, the model fails to predict the pH-dependent limiting values at low and high [KCl].

https://dx.doi.org/10.1021/acs.langmuir.0c01694
Langmuir XXXX, XXX, XXX−XXX

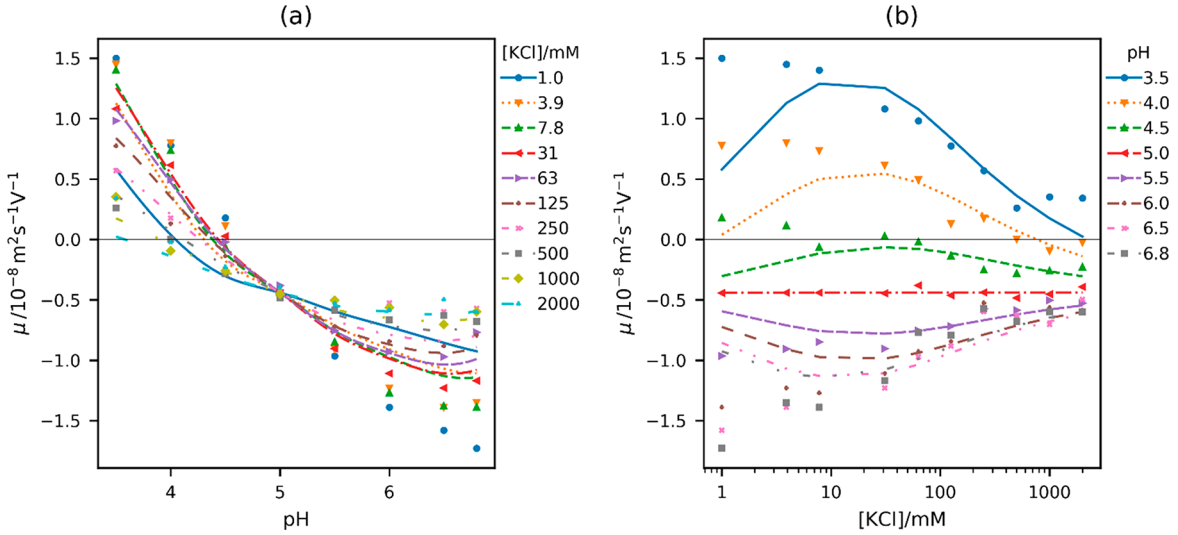

Figure 11. Electrophoretic mobility (a) as a function of pH (grouped by [KCl]) and (b) as a function of [KCl] (grouped by pH). Datum markers are experimental data. Lines show the fit to the Ohshima overlapping double layer model (eq 24).

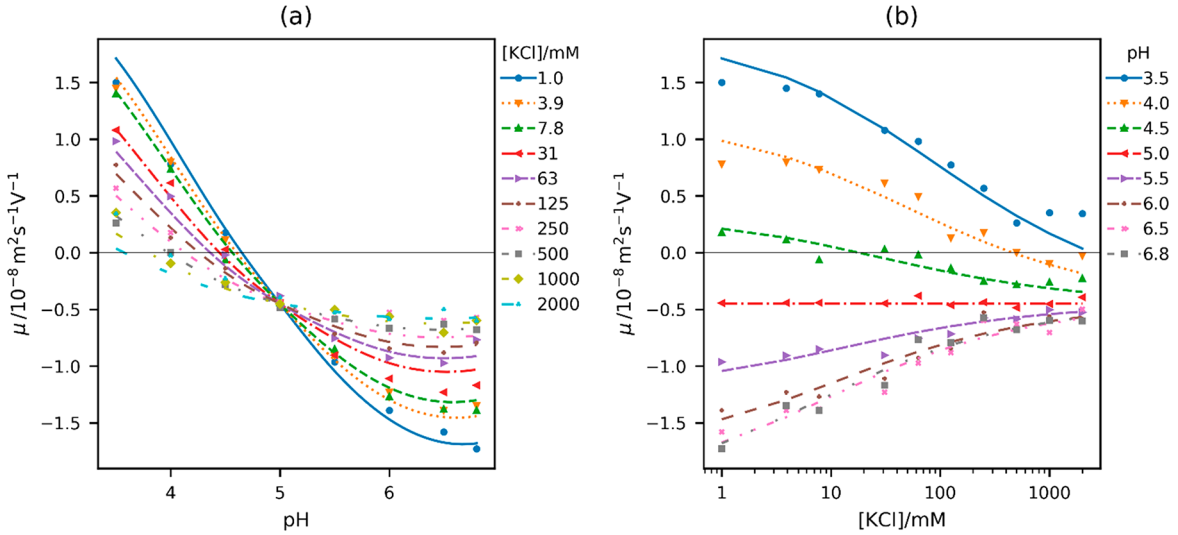

Figure 12. Electrophoretic mobility (a) as a function of pH (grouped by [KCl]) and (b) as a function of [KCl] (grouped by pH). Datum markers are experimental data. Lines show the fit to the Henry model (eq 11) with compensation for an increased number of counterions bound to each protein molecule at pH ≤ 4.5 compared to that at the iip.

Hermans Model. Figure 10 shows the comparison between the experimental electrophoretic mobility data (datum markers) and the predicted electrophoretic mobility (lines) according to the Hermans model (eq 19). The values of a and λ at each pH were estimated using the same procedure as for the Henry model (Figure 9).

In contrast to the Henry model, the Hermans model correctly predicts the limiting behavior of electrophoretic mobility above physiological ionic strengths as expected for a polyelectrolyte in aqueous solution. However, as with the Henry model, the Hermans model fails to predict the limiting behavior of electrophoretic mobility at low ionic strengths (<10 mM), notably at pH ≤ 4.0. Nevertheless, the mean values across all pHs for a and $1/\lambda$ obtained using the nonlinear least-squares analysis (3.0 ± 0.7 nm and 0.5 ± 0.2 nm, respectively) are consistent with the expected values for a globular protein.

As described in the Introduction, two mechanisms may yield measured electrophoretic mobilities at low [KCl] less than those predicted by either the Henry or Hermans models. The first mechanism is the interaction of double layers between neighboring protein molecules at sufficiently high protein concentration (eq 24), and the second mechanism is the increase in the number of chloride ions bound to protein molecules with decreasing pH of the solution.

Ohshima Overlapping Double Layers Model. Figure 11 shows the comparison between the experimental electrophoretic mobility data (datum markers) and the predicted electrophoretic mobility (lines) according to the Ohshima overlapping double layer model (eq 24) with $\phi \sim 0.05$. The values of a at each pH were estimated using the same procedure as for the Henry model (Figure 9).

Clearly, the model overemphasizes the reduction in electrophoretic mobility at [KCl] < 10 mM. Because the model assumes rigid, impermeable particles, it also fails to predict the limiting electrophoretic mobility above physiological ionic strengths. Assuming that the double layer interaction between hard particles is the same as between soft particles, it may be concluded that double layer interaction is unlikely to be

https://dx.doi.org/10.1021/acs.langmuir.0c01694
Langmuir XXXX, XXX, XXX−XXX

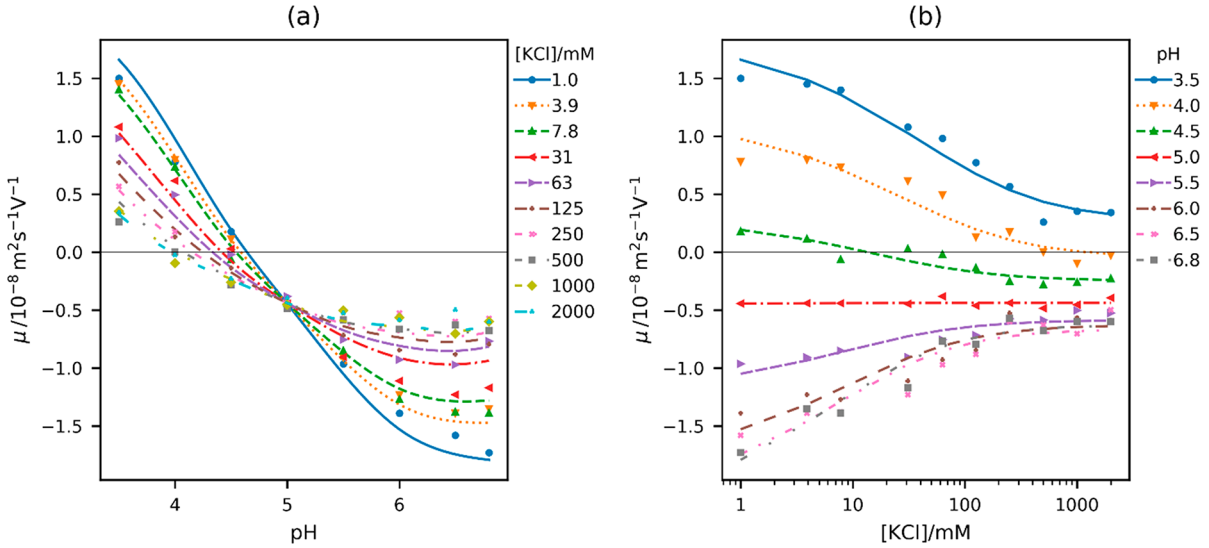

Figure 13. Electrophoretic mobility (a) as a function of pH (grouped by [KCl]) and (b) as a function of [KCl] (grouped by pH). Datum markers are experimental data. Lines show the fit to the Hermans model (eq 19) with compensation for an increased number of counterions bound to each protein molecule at pH ≤ 4.5 compared to that at the iip.

responsible for the reduction in electrophoretic mobility at low ionic strength. A similar model but for soft particles or polyelectrolytes is required to assess the presence of double layer interactions in protein solutions.

pH-Dependent Chloride Binding. The data analysis method described above assumes that the number of chloride ions binding to each protein molecule is independent of pH and equivalent to the number of elemental charges required to yield the electrophoretic mobility observed at the iip. Applying eq 11 yields an estimate of the number of chloride ions bound to each protein molecule to be 1.7 ± 0.4. This compares favorably with the result of 1.4 obtained by Scatchard et al. at the iip observed for the present study.

Increasing the number of bound chloride ions per protein molecule used to estimate electrophoretic mobilities at pHs 3.5, 4.0, and 4.5 by 18, 7 and 1, respectively, significantly improves the accuracy of the predicted electrophoretic mobilities for both the Henry model (Figure 12) and Hermans model (Figure 13). These estimates of the number of bound chloride ions are in reasonable semiquantitative agreement with the observations of Scatchard et al. for sodium chloride binding with bovine serum mercaptalbumin.

CONCLUSIONS

This paper has described a detailed investigation of the electrokinetic and electrostatic behaviors of BSA dissolved in aqueous potassium chloride solution at a wide range of acidities and ionic strengths. It has been shown that the methodologies commonly used by commercial ELS instruments are inappropriate for reliable characterization of the electrokinetic properties of proteins in free solution. The selection of electrode material is critical. Only platinized platinum electrodes should be used. Platinum and palladium electrodes (both of which are used in commercial instruments) must be avoided for measurements at physiological ionic strengths and higher. Expression of ELS data as zeta potentials should be avoided due to the "soft" nature of protein molecules in solution. Instead, data should be expressed either as electrophoretic mobilities or electrophoretic charges. Because the electrophoresis of proteins in solution depends on the net contribution of protonic and nonprotonic charges, it is important to quantify the contributions to the electrophoretic behavior by both types of charge. This is only possible by measuring electrophoretic mobilities at a suitable combination of pHs and ionic strengths. It has been shown that the small size of free protein molecules requires measurements at ionic strengths significantly higher and lower than for physiological conditions to determine the most appropriate electrokinetic model to use to estimate the protein charge. This work used protonic charge data obtained by potentiometric acid titration to assess the accuracy of predicting the experimentally observed electrophoretic mobilities using three separate electrokinetic models from which it is clear that the most frequently adopted electrokinetic models, such as the Henry model, should be avoided. Further, it is possible to conclude that BSA molecules in free solution behave as permeable polyelectrolytes and that there is a pH-dependent binding of chloride ions to the protein molecules.

AUTHOR INFORMATION

Corresponding Author

John F. Miller − *Enlighten Scientific LLC, Hillsborough, North Carolina 27278, United States;* orcid.org/0000-0001-6628-530X; Phone: +1 919 749 2800; Email: john@enlightenscientific.com

Complete contact information is available at: https://pubs.acs.org/10.1021/acs.langmuir.0c01694

Notes

The author declares no competing financial interest.

ACKNOWLEDGMENTS

Dr. David Fairhurst (Colloid Consultants Ltd.) is thanked for reviewing the manuscript and technical discussions. Dr. Michael Franklin (Research Triangle Institute International) is thanked for assistance in performing the EDS/SEM measurements.

REFERENCES

(1) Kim, B. Y. S.; Rutka, J. T.; Chan, W. C. W. Nanomedicine. *N. Engl. J. Med.* **2010**, *363* (25), 2434−2443.

https://dx.doi.org/10.1021/acs.langmuir.0c01694
Langmuir XXXX, XXX, XXX−XXX

(2) MaHam, A.; Tang, Z.; Wu, H.; Wang, J.; Lin, Y. Protein-Based Nanomedicine Platforms for Drug Delivery. *Small* **2009**, *5* (15), 1706−1721.
(3) Boisselier, E.; Astruc, D. Gold-Nanoparticles in Nanomedicine: Preparations, Imaging, Diagnostics, Therapies and Toxicity. *Chem. Soc. Rev.* **2009**, *38* (6), 1759−1782.
(4) Wang, Y.; Chen, L. Quantum-Dots, Lighting up the Research and Development of Nanomedicine. *Nanomedicine* **2011**, *7* (4), 385−402.
(5) Gessner, A.; Lieske, A.; Paulke, B.-R.; Müller, R. H. Functional-Groups on Polystyrene Model Nanoparticles: Influence on Protein Adsorption. *J. Biomed. Mater. Res., Part A* **2003**, *65A* (3), 319−326.
(6) *Polymers at Interfaces*, 1st ed.; Fleer, G. J., Ed.; Chapman & Hall: London, 1993.
(7) Fleer, G. J.; Lyklema, J. Forces-and Mechanisms in the Adsorption of Uncharged and Ionizable Macromolecules and of Proteins. *Makromol. Chem., Macromol. Symp.* **1988**, *17* (1), 39−56.
(8) Lassen, B.; Malmsten, M. Competitive-Protein Adsorption at Plasma Polymer Surfaces. *J. Colloid Interface Sci.* **1997**, *186* (1), 9−16.
(9) Lyklema, J. Proteins-at Solid—Liquid Interfaces A Colloid-Chemical Review. *Colloids Surf.* **1984**, *10*, 33−42.
(10) Norde, W. Driving-Forces for Protein Adsorption at Solid Surfaces. *Macromol. Symp.* **1996**, *103* (1), 5−18.
(11) Norde, W.; Lyklema, J. Interfacial-Behaviour of Proteins, with Special Reference to Immunoglobulins. A Physicochemical Study. *Adv. Colloid Interface Sci.* **2012**, *179*−*182*, 5−13.
(12) Lemp, J. F.; Asbury, E. D.; Ridenour, E. O. Electrophoresis-of Colloidal Biological Particles. *Biotechnol. Bioeng.* **1971**, *13* (1), 17−47.
(13) Loeb, J. Stability-of Suspensions of Solid Particles of Proteins and Protective Action of Colloids. *J. Gen. Physiol.* **1923**, *5* (4), 479−504.
(14) Rothen, A.; Mathot, C. Immunological Reactions Carried Out at a Liquid-Solid Interface with the Help of a Weak Electric Current. In *Surface Chemistry of Biological Systems*; Blank, M., Ed.; Springer US: Boston, MA, 1970; Vol. 7, pp 209−216, DOI: 10.1007/978-1-4615-9005-7_12.
(15) Abramson, H. A. Electrokinetic-Phenomena: VI. Relationship Between Electric Mobility, Charge, and Titration of Proteins. *J. Gen. Physiol.* **1932**, *15* (5), 575−603.
(16) Cedervall, T.; Lynch, I.; Lindman, S.; Berggard, T.; Thulin, E.; Nilsson, H.; Dawson, K. A.; Linse, S. Understanding-the Nanoparticle-Protein Corona Using Methods to Quantify Exchange Rates and Affinities of Proteins for Nanoparticles. *Proc. Natl. Acad. Sci. U. S. A.* **2007**, *104* (7), 2050−2055.
(17) Cedervall, T.; Lynch, I.; Foy, M.; Berggård, T.; Donnelly, S. C.; Cagney, G.; Linse, S.; Dawson, K. A. Detailed-Identification of Plasma Proteins Adsorbed on Copolymer Nanoparticles. *Angew. Chem., Int. Ed.* **2007**, *46* (30), 5754−5756.
(18) Darabi Sahneh, F.; Scoglio, C.; Riviere, J. Dynamics-of Nanoparticle-Protein Corona Complex Formation: Analytical Results from Population Balance Equations. *PLoS One* **2013**, *8* (5), No. e64690.
(19) Gebauer, J. S.; Malissek, M.; Simon, S.; Knauer, S. K.; Maskos, M.; Stauber, R. H.; Peukert, W.; Treuel, L. Impact-of the Nanoparticle-Protein Corona on Colloidal Stability and Protein Structure. *Langmuir* **2012**, *28* (25), 9673−9679.
(20) Ke, P. C.; Lin, S.; Parak, W. J.; Davis, T. P.; Caruso, F. A-Decade of the Protein Corona. *ACS Nano* **2017**, *11* (12), 11773−11776.
(21) Lundqvist, M.; Stigler, J.; Elia, G.; Lynch, I.; Cedervall, T.; Dawson, K. A. Nanoparticle-Size and Surface Properties Determine the Protein Corona with Possible Implications for Biological Impacts. *Proc. Natl. Acad. Sci. U. S. A.* **2008**, *105* (38), 14265−14270.
(22) Lynch, I.; Dawson, K. A. Protein-Nanoparticle Interactions. *Nano Today* **2008**, *3* (1), 40−47.
(23) Monopoli, M. P.; Walczyk, D.; Campbell, A.; Elia, G.; Lynch, I.; Baldelli Bombelli, F.; Dawson, K. A. Physical-Chemical Aspects of Protein Corona: Relevance to in Vitro and in Vivo Biological Impacts of Nanoparticles. *J. Am. Chem. Soc.* **2011**, *133* (8), 2525−2534.
(24) Walkey, C. D.; Chan, W. C. W. Understanding-and Controlling the Interaction of Nanomaterials with Proteins in a Physiological Environment. *Chem. Soc. Rev.* **2012**, *41* (7), 2780−2799.
(25) Dobiáš, B.; Qiu, X.; von Rybinski, W. *Solid-Liquid Dispersions*; Surfactant Science Series; Marcel Dekker: New York, 1999.
(26) Myers, D. *Surfaces, Interfaces, and Colloids: Principles and Applications*, 2nd ed.; Wiley-VCH: New York, 1999.
(27) Mysels, K. J. *Introduction to Colloid Chemistry*; Krieger: Huntington, NY, 1959.
(28) Verwey, E. J. W. Theory-of the Stability of Lyophobic Colloids. *J. Phys. Colloid Chem.* **1947**, *51* (3), 631−636.
(29) Verwey, E. J. W.; Overbeek, J. T. G. *Theory of the Stability of Lyophobic Colloids*; Dover Publications: Mineola, NY, 1948.
(30) Sjöqvist, J. Physiologisch-Chemische Beobachtungen Über Salzsäure [1]. *Skand. Arch. Physiol.* **1894**, *5* (1), 277−376.
(31) Wooley, J. C.; Ye, Y. A Historical Perspective and Overview of Protein Structure Prediction. In *Computational Methods for Protein Structure Prediction and Modeling: Vol. 1: Basic Characterization*; Xu, Y., Xu, D., Liang, J., Eds.; Biological and Medical Physics Biomedical Engineering; Springer New York: New York, NY, 2007; pp 1−43, DOI: 10.1007/978-0-387-68372-0_1.
(32) Nelson, D. L.; Cox, M. M.; Lehninger, A. L. *Lehninger Principles of Biochemistry*, 7th ed.; W. H. Freeman and Company; Macmillan Higher Education: New York, NY; Houndmills, Basingstoke, 2017.
(33) Hass, M. A. S.; Mulder, F. A. A. Contemporary-NMR Studies of Protein Electrostatics. *Annu. Rev. Biophys.* **2015**, *44* (1), 53−75.
(34) Sørensen, S. P. L.; Linderstrøm-Lang, K.; Lund, E. The-Influence of Salts upon the Ionisation of Egg Albumin. *J. Gen. Physiol.* **1927**, *8* (6), 543−599.
(35) Bryan, W. P. The-Isoionic Point of Amino Acids and Proteins. *Biochem. Educ.* **1978**, *6* (1), 14−15.
(36) Hunter, R. J. *Zeta Potential in Colloid Science: Principles and Applications*; Colloid Science: A Series of Monographs; Academic Press: London, 1981.
(37) Bier, M. *Electrophoresis: Theory, Methods, and Applications*; Elsevier, 2013.
(38) Swan, J. W.; Furst, E. M. A-Simpler Expression for Henry's Function Describing the Electrophoretic Mobility of Spherical Colloids. *J. Colloid Interface Sci.* **2012**, *388* (1), 92−94.
(39) Medda, L.; Barse, B.; Cugia, F.; Boström, M.; Parsons, D. F.; Ninham, B. W.; Monduzzi, M.; Salis, A. Hofmeister-Challenges: Ion Binding and Charge of the BSA Protein as Explicit Examples. *Langmuir* **2012**, *28* (47), 16355−16363.
(40) Baler, K.; Martin, O. A.; Carignano, M. A.; Ameer, G. A.; Vila, J. A.; Szleifer, I. Electrostatic-Unfolding and Interactions of Albumin Driven by PH Changes: A Molecular Dynamics Study. *J. Phys. Chem. B* **2014**, *118* (4), 921−930.
(41) Popovic, D. *Modeling of Conformation and Redox Potentials of Hemes and Other Cofactors in Proteins*. Ph.D. Thesis, Freie Universität Berlin, Berlin, Germany2002.
(42) Estévez, R.; Jentsch, T. CLC-Chloride Channels: Correlating Structure with Function. *Curr. Opin. Struct. Biol.* **2002**, *12* (4), 531−539.
(43) Scatchard, G.; Coleman, J. S.; Shen, A. L. Physical-Chemistry of Protein Solutions. VII. The-Binding of Some Small Anions to Serum Albumin. *J. Am. Chem. Soc.* **1957**, *79* (1), 12−20.
(44) Ohshima, H. Electrophoretic-Mobility of Soft Particles. *Electrophoresis* **1995**, *16* (1), 1360−1363.
(45) Allison, S. A. Modeling-the Electrophoresis of Rigid Polyions. Inclusion of Ion Relaxation. *Macromolecules* **1996**, *29* (23), 7391−7401.
(46) Chae, K. S.; Lenhoff, A. M. Computation-of the Electrophoretic Mobility of Proteins. *Biophys. J.* **1995**, *68* (3), 1120−1127.
(47) Duval, J. F. L.; Ohshima, H. Electrophoresis-of Diffuse Soft Particles. *Langmuir* **2006**, *22* (8), 3533−3546.
(48) Fujita, H. Notes-on the Calculation of Electrophoresis of Polyelectrolytes with Partial Free-Drainage. *J. Phys. Soc. Jpn.* **1957**, *12* (8), 968−973.
(49) Hermans, J. J. Sedimentation-and Electrophoresis of Porous Spheres. *J. Polym. Sci.* **1955**, *18* (90), 527−534.
(50) Hsu, H.-P.; Lee, E. Electrophoresis-of a Single Charged Porous Sphere in an Infinite Medium of Electrolyte Solution. *J. Colloid Interface Sci.* **2013**, *390* (1), 85−95.

https://dx.doi.org/10.1021/acs.langmuir.0c01694
Langmuir XXXX, XXX, XXX−XXX

(51) Kim, J. Y.; Ahn, S. H.; Kang, S. T.; Yoon, B. J. Electrophoretic-Mobility Equation for Protein with Molecular Shape and Charge Multipole Effects. *J. Colloid Interface Sci.* **2006**, *299* (1), 486−492.
(52) Makino, K.; Ohshima, H. Soft-Particle Analysis of Electrokinetics of Biological Cells and Their Model Systems. *Sci. Technol. Adv. Mater.* **2011**, *12* (2), 023001.
(53) Yeh, L.-H.; Liu, K.-L.; Hsu, J.-P. Importance of Ionic Polarization Effect on the Electrophoretic Behavior of Polyelectrolyte Nanoparticles in Aqueous Electrolyte Solutions. *J. Phys. Chem. C* **2012**, *116* (1), 367−373.
(54) Hermans, J. J.; Fujita, H. Electrophoresis-of Charged Polymer Molecules with Partial Free Drainage. *Konikl. Ned. Akad. Wetenschap. Proc.* **1955**, *B58*, 182−187.
(55) Debye, P.; Bueche, A. M. Intrinsic-Viscosity, Diffusion, and Sedimentation Rate of Polymers in Solution. *J. Chem. Phys.* **1948**, *16* (6), 573−579.
(56) Ohshima, H. Electrophoretic-Mobility of Spherical Colloidal Particles in Concentrated Suspensions. *J. Colloid Interface Sci.* **1997**, *188* (2), 481−485.
(57) Feltham, A. M.; Spiro, M. Platinized-Platinum Electrodes. *Chem. Rev.* **1971**, *71* (2), 177−193.
(58) Miller, J. F. *The Determination of Very Small Electrophoretic Mobilities in Polar and Nonpolar Colloidal Dispersions Using Phase Analysis Light Scattering*. Ph.D. Thesis, University of Bristol, Bristol, U.K., 1990.
(59) Miller, J. F.; Schätzel, K.; Vincent, B. The-Determination of Very Small Electrophoretic Mobilities in Polar and Nonpolar Colloidal Dispersions Using Phase Analysis Light Scattering. *J. Colloid Interface Sci.* **1991**, *143* (2), 532−554.
(60) Uzgiris, E. E. Laser-Doppler Methods in Electrophoresis. *Prog. Surf. Sci.* **1981**, *10* (1), 53−164.
(61) Miller, J. F. *Measuring Electrophoretic Mobility*. U.S. Patent 10,690,625, June 23, 2020.
(62) Salis, A.; Boström, M.; Medda, L.; Cugia, F.; Barse, B.; Parsons, D. F.; Ninham, B. W.; Monduzzi, M. Measurements-and Theoretical Interpretation of Points of Zero Charge/Potential of BSA Protein. *Langmuir* **2011**, *27* (18), 11597−11604.
(63) *AN199 - Zeta potential of proteins*. https://static.horiba.com/fileadmin/Horiba/Application/Health_Care/Biochemistry/AN199_Zeta_Potential_of_Proteins.pdf (accessed 2019-09-06).
(64) *AN110708 - Improving Protein Zeta Potential Measurements Utilizing A Novel Diffusion Barrier technique*. https://www.malvernpanalytical.com/en/learn/knowledge-center/application-notes/AN110708NovelDiffusionBarrierTechnique (accessed 2019-09-06).
(65) *AN120912 - Measurements of protein electrophoretic mobility using the Zetasizer Nano ZSP*. https://www.malvernpanalytical.com/en/learn/knowledge-center/application-notes/AN120912ProteinElectrophoreticMobility (accessed 2019-09-06).

https://dx.doi.org/10.1021/acs.langmuir.0c01694
Langmuir XXXX, XXX, XXX−XXX